

A Nonlinear Optimization Model for Transient Stable Line Switching

Terrence W.K. Mak, Pascal Van Hentenryck, and Ian A. Hiskens

Abstract—Transmission line switching is an important operational action in power transmission systems, and has been successfully applied to reduce generation costs and eliminate congestions. Prior work mainly focus on tackling the Optimal Transmission Switching problem based on steady states. This paper studies how to generalize these results when transmission switching is performed on highly congested systems. It proposes an optimization model to find the optimal line to switch and the corresponding optimal control parameters. The results show that optimizing the exciter and stabilizer control settings is critical to ensure stability and the optimization model can be solved within a few minutes. The model was validated with respect to a simulation model and is shown to an accuracy in the order of 10^{-3} (deg) accurate in rotor angle computations.

Index Terms—power systems, line switching, transient stability, optimal control, optimization, power system stabilizer

I. INTRODUCTION

Transmission line switching is a control action in electrical power systems that has generated increasing attention in recent years. Opening and closing transmission lines change the topology of the grid, redistribute power flows and change the operational state of the system. The control action has been proposed to address voltage issues in the grid, reduce generation costs [1]–[3], eliminate congestions, and avoid violating operational constraints [4].

Significant research has devoted to designing algorithms for Optimal Transmission Switching (OTS) [3]. The goal in OTS is to find the best (sequence of) lines to switch off in order to minimize generation costs. This line of research almost exclusively focuses on analyzing the power flow in the steady-states before and after the switchings. From a mathematical standpoint, the OTS problem for finding the optimal line(s) for single/multiple line switching(s) is a non-convex Mixed-Integer Non-Linear Program (non-convex MINLP), which is computationally challenging. For this reason, most OTS studies replace the non-convex AC power flow equations by the linear DC power flow equations [3], [5]–[8]. This reduces the computational complexity, as the DC-OTS problem can be modeled as a Mixed-Integer Linear Program (MILP). Unfortunately, there is no guarantee that the resulting solution can be transformed into an AC-feasible solution [9]. To overcome this limitation, recent work has advocated the use of AC formulations (AC-OTS) or the use of tighter approximations and relaxations [1], [2], [10].

T.W.K. Mak is affiliated with both Data61 in CSIRO, Australian National University, and University of Michigan. Terrence.Mak@data61.csiro.au

P. Van Hentenryck is affiliated with Department of IOE, University of Michigan. pvanhent@umich.edu

I.A. Hiskens is affiliated with Department of EECS, University of Michigan. hiskens@umich.edu

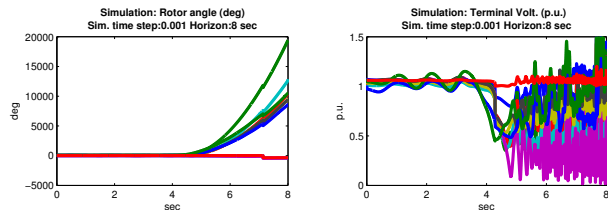


Fig. 1. Rotor angles (deg, left) and terminal voltage (p.u., right) for 88% congestion level on NESTA `nesta_case39_epri_api`.

AC-OTS formulations produce an optimal AC-feasible steady state after switchings, but do not guarantee transient stability when the congestion level goes beyond traditional $n-1$ reliability analysis. Our simulation experiments on the IEEE-39 test case indicate the more congested the network is, the more difficult it becomes to ensure transient stability of OTS. Figure 1 depicts simulation results when line (2,25) is open for a congested case of the IEEE 39-bus test system [11], [12] taken from [13]. In the first few seconds, the system seems to maintain stability. However, the system is insufficiently damped, causing oscillatory instability (slipping of generator poles). A loss of generator synchronism (the left plot) can be seen after the fifth second. Power utilities routinely check system stability under peak loads, via simulations on various faulty scenarios (e.g. single line / three phase faults). However, these routines are not exhaustive and mainly served for instability prevention during faults. With growing penetration of renewable energy, transmission switching is often presented as a flexible control action and it becomes important to have automatic routines and controllers that jointly optimize operational decisions and control settings.

This paper is a step in remedying this situation. It proposes an automatic routine which actively considered transient stability during optimization. Its key contribution is a nonlinear optimization model for Transient-Stable Line Switching (TSLs) whose role is to complement an AC-OTS model: For each contemplated line switching, the TSLs model determines set-points for its control variables in order to ensure transient stability or determine transient instability, in which case the switching is rejected. The TSLs optimization model uses a trapezoidal discretization of the differential algebraic equations for a 2-axis generator model with an automatic voltage regulator (AVR) consisting of an exciter and a stabilizer. The TSLs model features two types of control variables: generation dispatches and excitation parameters, and its objective function minimizes the rotor angle accelerations weighted by time in order to damp and stabilize the system.

The TSLS model was evaluated on the classical IEEE 10-machine 39-bus system [11], [12] with different congestion scenarios from the NESTA benchmark [13] to capture peaks in demand. The key findings from the experiments can be summarized as follows:

- 1) The more congested the system is, the more difficult it is to ensure transient stability.
- 2) The variables controlling the set-points of the exciter and the stabilizer are critical to ensure transient stability. With fixed constants for these parameters, transient stability cannot be obtained for the most congested case.
- 3) The TSLS optimization results were validated against POWERWORLD simulations and exhibits an average error in the order of 10^{-3} degree for rotor angles.
- 4) The TSLS optimization model is solved with one minute for the coarser, but highly accurate, discretization.

These results seem to indicate that optimal transient-stable line switching may become a practical tool for deploying line switching, complementing the significant progress achieved in the last decade.

II. RELATED WORK

Our work is closely related to the transient-stable optimal power flow problem, first proposed by Gan et al. [14]. The problem was later extended to multi-contingency settings in [15] and extended to power system restorations [16]. All of the above approaches utilize the classical model with Swing equations to reason on transient stability. Our work extends these works by further considering the more complex 2-Axis Model with automatic voltage regulation (AVR): including an exciter and a stabilizer (PSS) during optimization. Our work is also related to techniques improving stability during transmission loop closures in normal operating conditions, e.g., techniques on reducing rotor shaft impacts and standing phase angles [17]–[19].

III. BACKGROUND

The dynamic response of a power system after a disturbance can be abstractly written and described by [15], [21]:

$$\dot{x} = f(x, y), \quad 0 = g(x, y) \quad (1)$$

where $f(\bullet)$ represents a set of first-order differential equations describing the power system dynamics, and $g(\bullet)$ represents a set of algebraic equations describing the passive equipments. Vector x captures the short-term dynamic variables and y is a vector of algebraic state variables. Given an initial condition for variables x and y , we then compute the transient states of the network over time.

In this paper, we mainly focus on generator electro-mechanical dynamics and phenomenon within a time horizon from a few seconds up to half of a minute. The remaining equipments in the power transmission network, including transmission lines, circuit breakers, and loads are modeled as passive equipments. We now describe the technical details of the generator dynamics in our model.

A. Generator Model: 2-Axis Model

This paper uses the two-axis model [22] to capture the generator swing dynamics, starting with the swing equations:

$$\frac{d\delta^i}{dt} = \omega^i - \omega^0, \quad \frac{2H^i}{\omega^0} \frac{d\omega^i}{dt} = p_m^i - p_e^i - D^i \omega^i$$

where H^i , δ^i , D^i , ω^i , and ω^0 denote the inertia constant, rotor angle, the damping coefficient, the angular velocity, and the nominal angular velocity of a generator i . The nominal angular velocity is assumed constant for all generators at 60Hz (i.e., $\omega^0 = 2\pi 60$). p_m^i and p_e^i represent the mechanical and electrical powers acting on the rotor of generator i , δ^i and ω^i are short-term dynamic variables, and p_m^i and p_e^i are algebraic state variables. In steady states, the mechanical power is assumed to be equal to the electrical power and the rotor angles of all generators remain constant (i.e., $\frac{d\omega^i}{dt} = 0, \forall i \in G$). The angular velocity ω^i is traditionally defined as an offset with respect to the nominal angular velocity ω^0 , which allows us to drop the ω^0 term (first equation). Traditionally, D is an implicit constant use to approximate damping effects on windings and stabilizers. Since our model includes an exciter and a stabilizer, the term $D^i \omega^i$ in the second equation can be ignored. In the two-axis model, the active (p_e^i) and reactive (q_e^i) power of generator i can be described directly in terms of the generator stator emfs, leading to rotor flux components in two axes: the direct axis (d-axis, E_d^i) and the quadrature axis (q-axis, E_q^i):

$$p_e^i = \frac{E_q^i V^i \sin(\delta^i - \theta^i)}{X_d^i} + \frac{E_d^i V^i \cos(\delta^i - \theta^i)}{X_q^i} + \frac{(V^i)^2 (X_d^i - X_q^i) \sin(2\delta^i - 2\theta^i)}{2X_d^i X_q^i}$$

$$q_e^i = -\frac{(V^i)^2}{X_d^i} + \frac{E_q^i V^i \cos(\delta^i - \theta^i)}{X_d^i} - \frac{E_d^i V^i \sin(\delta^i - \theta^i)}{X_q^i} + \frac{(V^i)^2 (E_d^i - E_q^i) (\cos(2\delta^i - 2\theta^i) - 1)}{2X_d^i X_q^i}$$

where E_q^i , E_d^i , V^i , θ^i , X_d^i , and X_q^i are the q-axis stator emf, d-axis stator emf, terminal bus voltage (magnitude), the bus phase angle, d-axis transient reactance, and q-axis transient reactance of generator i respectively. The dynamics of the two stator emfs E_q^i and E_d^i are further described by:

$$T_{do}^i \frac{dE_q^i}{dt} = E_{fd}^i - E_q^i + (X_d^i - X_q^i) I_d^i$$

$$T_{qo}^i \frac{dE_d^i}{dt} = -E_d^i + (X_q^i - X_d^i) I_q^i$$

where E_{fd}^i is the excitation field voltage controlled by the automatic voltage regulators (AVRs) and power system stabilizers (PSS), T_{do}^i and T_{qo}^i are the open circuit d- and q-axis time constants, X_d^i and X_q^i are the d- and q-axis synchronous reactance, and I_d^i and I_q^i are the d- and q-axis stator currents for generator i respectively. Finally, we have the following equations to link the stator currents to the

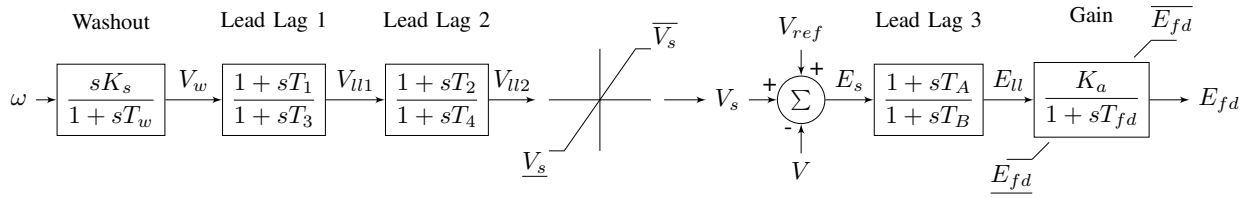


Fig. 2. The control block diagram of our automatic voltage regulator (AVR), with one exciter: SEXS.PTI [20] and one stabilizer: STAB1 [20]

terminal voltage and the stator emfs:

$$I_d^i = \frac{V^i \cos(\delta^i - \theta^i) - V_q^i}{X_d^i}, I_q^i = \frac{V^i \sin(\delta^i - \theta^i) + V_d^i}{X_q^i}$$

B. Automatic Voltage Regulation Model (AVR)

Our generator model implements a simplified excitation system model SEXS.PTI [20] combined with a speed-sensitive stabilizing model STAB1 [20]. Figure 2 shows the combined block diagram for all of the transfer functions in Laplace form. The circuit requires three external inputs: the terminal voltage V , the steady-state terminal voltage reference V_{ref} , and the angular velocity/speed of the rotor angle ω . The excitation circuit consists of three time constants: T_A and T_B in the lead-lag block and T_{fd} in the amplification block, one amplification gain parameter K_a and two limits $\overline{E_{fd}}$ and $\underline{E_{fd}}$ to avoid over-excitation. The speed-sensitive stabilizing circuit consists of 5 time constants: T_w in the wash out block and T_1 to T_4 in the two lead-lag block, one wash out gain constant K_s , and again two limits $\overline{V_s}$ and $\underline{V_s}$ to limit the stabilizing signal V_s .

IV. FINITE DIFFERENCE DISCRETIZATION

To optimize the 2-Axis model with the AVR containing ordinary differential equations, one method is to use direct time discretization method to convert the continuous optimization problem into a finite-time discretized nonlinear program. We follow previous work [14] and perform an implicit trapezoidal discretization to discretize the equations over a discrete horizon ($1 \leq t \leq T$). This approach discretizes the first-order differential equation

$$\frac{df(t)}{dt} = k(t)$$

over a finite discrete time horizon $1 \leq t \leq T$ with uniform time step Δ by converting it into its integral form

$$\int_t^{t+\Delta} \frac{df(t)}{dt} dt = f(t+\Delta) - f(t) = \int_t^{t+\Delta} k(t) dt$$

and using the Trapezoidal rule as follows:

$$\int_t^{t+\Delta} k(t) dt \approx \frac{\Delta}{2} [k(t) + k(t+\Delta)]$$

The same approximation is repeated to cover the required horizon and gives

$$f(t+1) - f(t) \approx \frac{\Delta}{2} [k(t) + k(t+1)], 1 \leq t \leq T-1$$

We now show the discretized formulations for building our optimization model. We append t within brackets to variables to denote the values of the variables at time step t and use $t|_{t=n}$ to refer to a specific time step n .

A. 2 Axis Model: Swing equations

The Swing equations then become

$$\delta^i(t+1) - \delta^i(t) - \frac{\Delta}{2} (\omega^i(t+1) + \omega^i(t)) = 0 \quad (2)$$

$$\omega^i(t+1) - \omega^i(t) - \frac{\Delta}{2} (a^i(t+1) + a^i(t)) = 0 \quad (3)$$

$$a^i(t) - \frac{\omega^0}{2H^i} (p_m^i - p_e^i(t)) = 0 \quad (4)$$

for all generator $i \in G$ and all time steps $t \in [1..T-1]$. The initial boundary conditions at $t = 1$ is given by

$$\omega^i(t|_{t=1}) = 0, a^i(t|_{t=1}) = 0, p_m^i = p_e^i(t|_{t=1}) \quad \forall i \in G. \quad (5)$$

by assuming steady state holds in the first time step ($t = 1$) and mechanical power is in balance with steady-state electrical power. To ensure rotor stability, one acceptable criteria [14] is to ensure that the rotor angles are not too far from each others before and after the disturbance period. One typical approach is to define a reference angle $\delta^r(t)$ representing the angle for the center of inertia (COI):

$$\delta^r(t) = \frac{\sum_{i \in G} H^i \delta^i(t)}{\sum_{i \in G} H^i}, \quad 1 \leq t \leq T. \quad (6)$$

For all generators i , the stability constraints then become

$$-\bar{\delta} \leq \delta^i(t) - \delta^r(t) \leq \bar{\delta}, \quad \{1\} \cup \{t : T_k \leq t \leq T\} \quad (7)$$

where T_k is an adjustable time constant representing the earliest time that the constraint has to be enforced (after switchings), and $\bar{\delta}$ is an adjustable parameter representing the maximum rotor angle separation. In the literature, $\bar{\delta}$ is usually set to $\pi/2$ (rad).

B. 2Axis Model: Generator Power

The generation active and reactive power can be easily extended to the discretized space by repeating the equations to all time steps t . For all $i \in G, t \in [1..T]$:

$$p_e^i(t) = \frac{E_q^i(t) V^i(t) \sin[\delta^i(t) - \theta^i(t)]}{X_d^i} + \frac{E_d^i(t) V^i(t) \cos[\delta^i(t) - \theta^i(t)]}{X_q^i} + \frac{[V^i(t)]^2 (X_d^i - X_q^i) \sin[2\delta^i(t) - 2\theta^i(t)]}{2X_d^i X_q^i} \quad (8)$$

$$q_e^i(t) = -\frac{[V^i(t)]^2}{X_d^i} + \frac{E_q^i(t) V^i(t) \cos[\delta^i(t) - \theta^i(t)]}{X_d^i} - \frac{E_d^i(t) V^i(t) \sin[\delta^i(t) - \theta^i(t)]}{X_q^i} + \frac{[V^i(t)]^2 [E_d^i(t) - E_q^i(t)] \{\cos[2\delta^i(t) - 2\theta^i(t)] - 1\}}{2X_d^i X_q^i} \quad (9)$$

C. 2Axis Model: Stator EMF Dynamics

Similarly, the d- and q-axis stator emf dynamics will be discretized to:

$$T_{do}^i E_q^i(t) = E_{fd}^i(t) - E_q^i(t) + (X_d^i - X_d^{\prime i}) I_d^i(t) \quad (10)$$

$$T_{qo}^i E_d^i(t) = -E_d^i(t) + (X_q^i - X_q^{\prime i}) I_q^i(t) \quad (11)$$

$$I_d^i(t) = \frac{V^i(t) \cos[\delta^i(t) - \theta^i(t)] - V_q^i(t)}{X_d^{\prime i}} \quad (12)$$

$$I_q^i(t) = \frac{V^i(t) \sin[\delta^i(t) - \theta^i(t)] + V_d^i(t)}{X_q^{\prime i}} \quad (13)$$

for all $i \in G, t \in [1..T]$, with the following trapezoidal rule to approximate the rate of the emf dynamics:

$$E_q^i(t+1) - E_q^i(t) - \frac{\Delta}{2} [E_q^{\prime i}(t+1) + E_q^{\prime i}(t)] = 0 \quad (14)$$

$$E_d^i(t+1) - E_d^i(t) - \frac{\Delta}{2} [E_d^{\prime i}(t+1) + E_d^{\prime i}(t)] = 0 \quad (15)$$

for all $i \in G, t \in [1..T-1]$. Similarly, we have the following initial boundary conditions at $t = 1$:

$$E_d^{\prime i}(t|_{t=1}) = 0, E_q^{\prime i}(t|_{t=1}) = 0, \quad \forall i \in G. \quad (16)$$

by assuming steady state in the first time step.

D. Automatic Voltage Regulator: Exciter

We now show how we transform the transfer functions (in Laplace domain) in our AVR into time-domain differential equations for optimization. Let $O(s)/O(t)$ and $I(s)/I(t)$ be the output function and input function in the Laplace (s) / time (t) domain. All of the transfer functions appearing in Figure 2 can be written in abstract form as¹:

$$\begin{aligned} \frac{K_m + sT_m}{K_n + sT_n} &= \frac{O(s)}{I(s)} \\ \iff s(I(s)T_m - O(s)T_n) &= O(s)K_n - I(s)K_m \\ \iff \frac{d}{dt}(I(t)T_m - O(t)T_n) &= O(t)K_n - I(t)K_m \\ \iff \frac{dX(t)}{dt} &= O(t)K_n - I(t)K_m, \end{aligned}$$

where $X(t)$ is defined as $I(t)T_m - O(t)T_n$. For lead-lag blocks and washout blocks, we have $K_m = K_n = 1$ and $K_n = 1, K_m = 0$. These dynamic equations reduce to:

$$\frac{dX(t)}{dt} = O(t) - I(t), \text{ and } \frac{dX(t)}{dt} = O(t)$$

For excitation amp. blocks, we have $K_n = 1, T_m = 0$:

$$\frac{dX(t)}{dt} = O(t) - K_m I(t), \text{ s.t. } X(t) = -T_n O(t)$$

As a result, the following equations describe the excitation circuits:

$$T_{fd}^i E_{fd}^i(t) = -E_{fd}^i(t) + K_a^i E_{il}^i(t) \quad (\text{Gain}) \quad (17)$$

$$X_{il}^i(t) = E_s^i(t) - E_{il}^i(t) \quad (\text{Lead-Lag}) \quad (18)$$

$$X_{il}^i(t) = T_B^i E_{il}^i(t) - T_A^i E_s^i(t) \quad (\text{Lead-Lag}) \quad (19)$$

$$E_s^i(t) = V_{ref}^i - V^i(t) + V_s^i(t) \quad (\text{Summation}) \quad (20)$$

¹The equivalence conditions described are based on the common assumption that the transfer functions are given with zero initial condition.

for all $i \in G, t \in [1..T]$, with the following trapezoidal rule to approximate the dynamics:

$$E_{fd}^i(t+1) - E_{fd}^i(t) - \frac{\Delta}{2} [E_{fd}^{\prime i}(t+1) + E_{fd}^{\prime i}(t)] = 0 \quad (21)$$

$$X_{il}^i(t+1) - X_{il}^i(t) - \frac{\Delta}{2} [X_{il}^{\prime i}(t+1) + X_{il}^{\prime i}(t)] = 0 \quad (22)$$

for all $i \in G, t \in [1..T-1]$. Again, we have the following initial boundary conditions at $t = 1$:

$$E_{fd}^{\prime i}(t|_{t=1}) = 0, X_{il}^{\prime i}(t|_{t=1}) = 0 \quad (23)$$

for all $i \in G$. The only equipment we remain to convert to the time domain is the non-windup limiters on the gain block. The limiters will change and set the differential $\frac{dE_{fd}}{dt}$ and the state E_{fd} when the state goes lower/higher than the lower/upper bounds, as follows:

$$\begin{aligned} \frac{dE_{fd}}{dt} &= 0 \wedge E_{fd} = \overline{E_{fd}}, \quad \text{if } E_{fd} \geq \overline{E_{fd}} \wedge \frac{dE_{fd}}{dt} \geq 0 \\ \frac{dE_{fd}}{dt} &= 0 \wedge E_{fd} = \underline{E_{fd}}, \quad \text{if } E_{fd} \leq \underline{E_{fd}} \wedge \frac{dE_{fd}}{dt} \leq 0 \end{aligned} \quad (24)$$

To implement the limiter (in time-domain) for optimization, binary/integer variables would need to be used, introducing significant computational complexity and making the approach intractable. One alternative is to enforce **stricter** bounds:

$$\underline{E_{fd}} \leq E_{fd}(t) \leq \overline{E_{fd}}, \quad \forall i \in G, 1 \leq t \leq T. \quad (25)$$

The resulting optimization will be more **conservative**, as it requires control settings that satisfy the tightened bounds.

E. Automatic Voltage Regulator: Stabilizer

By using similar transformation technique, we will have the following equations to describe our stabilizer (PSS):

$$X_w^i(t) = V_w^i(t) \quad (\text{Wash out}) \quad (26)$$

$$X_w^i(t) = K_s^i \omega^i(t) - T_w^i V_w^i(t) \quad (\text{Wash out}) \quad (27)$$

$$X_{il1}^i(t) = V_w^i(t) - V_{il1}^i(t) \quad (\text{Lead-Lag 1}) \quad (28)$$

$$X_{il1}^i(t) = T_3^i V_{il1}^i(t) - T_1^i V_w^i(t) \quad (\text{Lead-Lag 1}) \quad (29)$$

$$X_{il2}^i(t) = V_{il1}^i(t) - V_{il2}^i(t) \quad (\text{Lead-Lag 2}) \quad (30)$$

$$X_{il2}^i(t) = T_4^i V_{il2}^i(t) - T_2^i V_{il1}^i(t) \quad (\text{Lead-Lag 2}) \quad (31)$$

for all $i \in G, t \in [1..T]$, with the following trapezoidal rule:

$$X_w^i(t+1) - X_w^i(t) - \frac{\Delta}{2} [X_w^{\prime i}(t+1) + X_w^{\prime i}(t)] = 0 \quad (32)$$

$$X_{il1}^i(t+1) - X_{il1}^i(t) - \frac{\Delta}{2} [X_{il1}^{\prime i}(t+1) + X_{il1}^{\prime i}(t)] = 0 \quad (33)$$

$$X_{il2}^i(t+1) - X_{il2}^i(t) - \frac{\Delta}{2} [X_{il2}^{\prime i}(t+1) + X_{il2}^{\prime i}(t)] = 0 \quad (34)$$

for all $i \in G, t \in [1..T-1]$, with similar initial conditions:

$$X_w^{\prime i}(t|_{t=1}) = 0, X_{il1}^{\prime i}(t|_{t=1}) = 0, X_{il2}^{\prime i}(t|_{t=1}) = 0 \quad (35)$$

for all $i \in G$. We now show how to handle the limiters in the stabilizers. These are windup limiters (also called saturation limiters) for filtering and modifying signal V_s before inputting to the exciters. The limiters will change and set the state

V_s when the input state V_{ll2} goes lower/higher than the lower/upper bounds, as follows:

$$\begin{aligned} V_s &= \overline{V}_s, & \text{if } V_{ll2} &\geq \overline{V}_s \\ V_s &= \underline{V}_s, & \text{if } V_{ll2} &\leq \underline{V}_s \\ V_s &= V_{ll2}, & \text{otherwise} \end{aligned}$$

To implement this limiter for optimization and avoid integer variables, we again enforce the stricter bounds:

$$V_{ll2}^i(t) = V_s^i(t), \underline{V}_s^i \leq V_s^i(t) \leq \overline{V}_s^i, \quad \forall i \in G, 1 \leq t \leq T. \quad (36)$$

F. Power Network: AC Power Flow

It remains to link the AC power flow equations to the generator dynamics. The model states the active and reactive flow balance equations

$$\begin{aligned} \sum_{m \in G(n)} p_e^m(t) - \sum_{m \in O(n)} p_l^m - [V^n(t)]^2 g_s^n &= \sum_{m \in N(n)} p_{nm}(t) \\ \sum_{m \in G(n)} q_e^m(t) - \sum_{m \in O(n)} q_l^m + [V^n(t)]^2 b_s^n &= \sum_{m \in N(n)} q_{nm}(t) \end{aligned} \quad (37)$$

for all bus $n \in N$, where $p_e^m(t)$ and $q_e^m(t)$ are the active and reactive power of generator m , p_l^m and q_l^m are the active and reactive demands of load m , $[V^n(t)]^2 g_s^n$ and $[V^n(t)]^2 b_s^n$ describe the active and reactive power drawn by the bus shunt ($g_s^n + ib_s^n$) at bus n , and $p_{nm}(t)$ and $q_{nm}(t)$ are the active and reactive power flow from n to m (i.e. bus injections). We use $G(n)$, $O(n)$, and $N(n)$ to denote the set of generators, loads, and neighboring buses of bus n . In this work, we simplify our experiments and use constant active and reactive power loads to demonstrate our techniques. Note that we can easily extend our model with: impedance, current, or even dynamic loads (based on voltage/frequency) by adjusting and replacing the two terms: p_l^m and q_l^m . The AC power flow equations describing the power flow of a transmission line are then written as:

$$\begin{aligned} p_{nm}(t) &= z_{nm}(t) \left\{ \frac{g_{nm}}{Tl_{nm}} [V^n(t)]^2 - \frac{V^n(t)V^m(t)}{Tr_{nm}} [g_{nm} \cos(\Theta_{nm}(t)) + b_{nm} \sin(\Theta_{nm}(t))] \right\} \\ q_{nm}(t) &= z_{nm}(t) \left\{ -\frac{b_{nm} + (l_{nm}^c)/2}{Tl_{nm}} [V^n(t)]^2 - \frac{V^n(t)V^m(t)}{Tr_{nm}} [g_{nm} \sin(\Theta_{nm}(t)) - b_{nm} \cos(\Theta_{nm}(t))] \right\} \\ \text{s.t. } \Theta^{nm}(t) &= \theta^n(t) - \theta^m(t) + \phi^{nm} \end{aligned} \quad (38)$$

where $g_{nm} + ib_{nm}$ is the line admittance, l_{nm}^c is the line charge, and $z_{nm}(t)$ is an on-off variable to determine whether line (n, m) is opened or closed. We assume $z_{nm}(t) = z_{mn}(t)$ for every time step t . During implementation, they will be implemented as the same variable. ϕ^{nm} denotes the constant phase shift angle parameter (in radians) if transmission line (n, m) has a phase shift transformer. Note that phase shifting is directional, and therefore $\phi^{nm} = -\phi^{mn}$. Parameter $Tr_{nm} = Tr_{mn}$ denotes the off-nominal turns ratio of a transformer on line (n, m) . Tr_{nm} will be set to 1 if no transformer exist. Tl_{nm} is set to $[Tr_{nm}]^2$ if the transformer gains voltage from bus n to m ; and set to 1 otherwise.

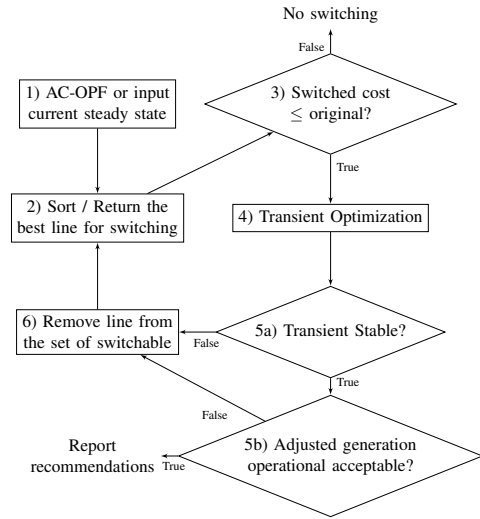


Fig. 3. Transient Stable Line Switching Algorithm

G. Power Network: Operational Limits

The active and reactive generation and line thermal/power limits for the initial steady state are given by

$$\underline{p}_e^i \leq p_e^i(t|_{t=1}) \leq \overline{p}_e^i \quad \forall i \in G \quad (39)$$

$$\underline{q}_e^i \leq q_e^i(t|_{t=1}) \leq \overline{q}_e^i \quad \forall i \in G \quad (40)$$

$$[p_{nm}(t|_{t=1})]^2 + [q_{nm}(t|_{t=1})]^2 \leq [\overline{S}_{nm}]^2 \quad \forall (n, m) \in L \quad (41)$$

where \overline{S}_{nm} denotes the maximum apparent power. We also enforce the following limits across all time steps t :

$$\underline{V}^n \leq V^n(t) \leq \overline{V}^n, \quad \forall n \in N \quad (42)$$

$$-\overline{\theta} \leq \delta^n(t) - \theta^n(t) \leq \overline{\theta}, \quad \forall n \in G \quad (43)$$

$$-\overline{\theta} \leq \theta^n(t) - \theta^m(t) \leq \overline{\theta}, \quad \forall (n, m) \in L \quad (44)$$

V. TRANSIENT STABLE LINE SWITCHING

This section presents our optimization model for transient-stable transmission line switching.

A. Line switching routine with transient stability

Figure 3 shows an automatic routine utilizing our proposed model to find the best transmission line to switch without causing transient instability.

- 1) The routine executes AC Optimal Power Flow algorithm (AC-OPF) to determine the current system state.
- 2) Based on the computed steady state, it finds the best line to switch (e.g., based on costs/congestions), e.g., by solving Model 1 in [1].
- 3) It checks whether the switched line reduces generation costs.
- 4) It then executes our model to search for a feasible optimal control solution to ensure finite-time transient stability when switching the proposed line.
- 5) It checks if the solution is transient stable and operationally acceptable.
- 6) If no feasible solution is found, the line will be discarded.

B. Transient optimization model

We now present the optimization model for Step 4:

Transient Stable Line Switching (TSLS)

$$\min \sum_{n \in G} \sum_{t \in [1, T]} [t(a^n(t))]^2 \quad (\text{O1})$$

s.t. Swing equations & stability: (2) – (7)
 Generator power: (8) – (9)
 Stator EMF dynamics: (10) – (16)
 Excitation dynamics: (17) – (25)
 PSS dynamics: (26) – (36)
 AC network power flow: (37) – (38)
 Operational limits: (39) – (44)
 Active power flexible region: $|p_e^i(t|_{t=1}) - p_T^i| \leq r p_T^i$
 Reactive power flexible region: $|q_e^i(t|_{t=1}) - q_T^i| \leq r q_T^i$
 Re-dispatch cost constraint: $c \leq (1 + \gamma)c_T$

where p_T^i and q_T^i are the active and reactive power of generator i in step 1, c and c_T are total generation costs of the current optimization problem and the generation costs in step 1. r and γ are adjustable parameters governing the maximum generator resources and maximum increase in generation costs allowed to achieve transient stability. Since our model could only guarantee stability within the computed horizon, solutions obtained from the model may not guarantee to be stable at any future time steps. One way to consider the stability continuity is to restrict our attention to solutions that provide enough damping and reduce the magnitude/amplitude of transient swings over time. The objective function (O1) minimizes the sum of time-weighted rotor angle accelerations, where the time-weights ensure that the solutions have smaller swings as time increases.

VI. COMPUTATIONAL CASE STUDY

This section evaluates the TSLS optimization model on the classical IEEE 10-machine 39-bus systems [11], [12] with the network data from Matpower [23]. The dynamics data (i.e., generator machine and AVR parameter) are obtained from a recent release (November 2013) of the IEEE PES Task Force on benchmark systems for stability controls [24]. To increase the difficulty of the test case, the computational results consider size congested scenarios from the NESTA test systems [13] (case `nesta_case39_eprl_api`) which increase the load by 50%, 70%, 80%, 85%, 88%, and 90%. To ease comparisons between different settings, the experiments assume that the proposed line switching occurs at time 0.002s. The TSLS model then considers a 4 second horizon, with stability parameters: $T_k = 3s$ and $\bar{\delta} = \frac{\pi}{2}$. The switching routine in Figure 3 is implemented in AMPL [25] and uses BONMIN 1.8.4 [26] with default MA27 [27] linear solver for steps 1 and 2. The TSLS optimization model in step 4 uses IPOPT 3.12.6 [28] compiled with an advanced linear solver HSL_MA77, designed for large scale systems by using an out-of-core multi-frontal method [27]. The computational studies explores two versions of the TSLS optimization model. The TSLS-G model use generator dispatches as its

TABLE I

RESULTS FOR THE TSLS-G MODEL: DISPATCH DISTANCE (MW/MVAR), COST DIFFERENCE (\$), AND RUNTIME (SEC).

Congestion (%)	Line	$r = 1\%, \gamma = 0.2\%$		
		Dispatch dist.	Cost diff.	Runtime
50	(4,14)	6.48/4.64	0.67 (0.02%)	81.10
70	(16,17)	13.98/7.59	1.84 (0.04%)	198.73
80	(16,17)	21.03/6.04	7.93 (0.15%)	96.83
85	(2,25)	7.96/5.58	0.70 (0.01%)	79.07
88	(16,17) ²	10.96/5.69	3.76 (0.06%)	294.01
90	No SW ⁴	Converge Err.	-	-

only control variables, while TSLS-PSS uses PSS controls (in the AVR circuit) instead of generation dispatches. Since time constants T_1 to T_4 (in PSS) are adjustable [29], the major difference between the TSLS-G and TSLS-PSS models is the fact that T_1 to T_4 are constants in TSLS-G and control variables in TSLS-PSS. In the experiments, T_1 and T_2 takes their values within [2, 5], and T_3 and T_4 within [0.02, 0.08] unless specified otherwise.

a) *Evaluation of the TSLS-G Model:* Table I presents the computational results for the TSLS-G model, including the proposed line for switching, the total CPU runtime, and two metrics to measure how much generation resource the model is used to achieve transient stability. The first metric is the generation differences (in L2 norm, MW/MVAR) with respect to the steady state:

$$\text{Active power (MW): } \sqrt{\sum_{n \in G} (p_e^i(t|_{t=1}) - p_T^i)^2}$$

$$\text{Reactive power (MVAR): } \sqrt{\sum_{n \in G} (q_e^i(t|_{t=1}) - q_T^i)^2}$$

The second metric is the increased cost (in dollars and percentage) due to the change in dispatch. When the first line proposed for switching (by Step 2 in Figure 3) is not transient stable, the table indicates the number of lines being checked in superscripts after the line results (see for instance the 88% case). Results are presented for $r = 1\%, \gamma = 0.2\%$. For low to mild congestion settings, the TSLS-G model verifies that the system with small changes to the generator dispatch (with costs $\leq 0.2\%$) ensures that the system is not unstable over the finite horizon considered after the line switching (i.e. all solved to locally optimal solution). When the congestion reaches 88%, the TSLS-G model could not find any stable generation dispatch within the 1% generation limit (i.e. infeasible), and therefore, the switching routine recommended the second best transmission line (16,17) to perform switching. When congestion level increases to 90%, the TSLS-G model could not find any transient-stable dispatches.

Solutions of the TSLS-G model are only stable in the fixed finite-time horizon and may become unstable in later time periods (i.e. after 4 sec). To verify the long-term stability of the TSLS-G solutions, a transient simulation on PowerWorld simulator (ver. 17) [20] (at 10^{-3} sec step size) was run on the 88% congestion case and initialized with the dispatch of the optimization model on opening line (16,17). Figure 4 presents the results. In particular, Figure 4 indicates that

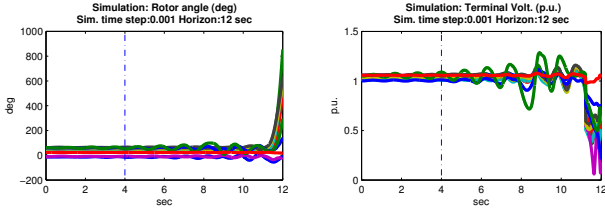


Fig. 4. TSLG Model: Rotor angles (deg) and terminal voltage (p.u.) for 88% congestion level ($r = 1\%$, $\gamma = 0.2\%$) on opening line (16,17).

TABLE II

RESULTS FOR THE TSLS-PSS MODEL: DISPATCH DISTANCE (MW/MVAR), COST DIFFERENCE (\$), AND RUNTIME (SEC).

Congestion (%)	No dispatch change: $r = 0\%$, $\gamma = 0.2\%$			
	Line	Dispatch dist.	Cost diff.	Runtime
50	(4,14)	0.00/0.00	0.00 (0.00%)	1206.84
70	(16,17)	0.00/0.00	0.00 (0.00%)	496.97
80	(16,17)	0.00/0.00	0.01(0.00%)	511.07
85	(2,25)	0.00/0.00	0.00 (0.00%)	239.08
88	(2,25)	0.00/0.00	0.00 (0.00%)	417.57
90	No SW ⁴	Converge Err.	-	-

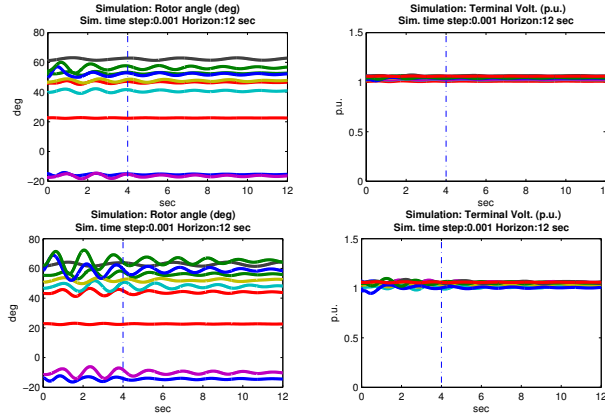


Fig. 5. TSLS-PSS Model: Rotor angles (deg) and terminal voltage (p.u.) with no dispatch change for opening line (2,25). Top: congestion level 85%, bottom: congestion level 88%

the TSLS-G model becomes unstable at about 11 seconds. Clearly, using only generator dispatch as control variables may not be sufficient to ensure long-term stability.

b) Evaluation of the TSLS-PSS Model: Table II presents the results of the TSLS-PSS model. The optimization model ensures the network is stable over the finite horizon for the recommended line switching and all congestion levels, except 90%. The simulation results, initialized with the AVR damping control, are shown in Figures 5 for congestion levels at 85% and 88%. They show a nice damping of rotor angles and stable voltage magnitudes, demonstrating the benefits of the model. Controlling the exciter/stabilizer settings is thus critical in using transmission line switching in highly congested situations and is a promising avenue for managing congestion.

c) Optimization Versus Simulation: It is interesting to compare the results of the TSLS-PSS model with a PowerWorld [20] simulation on the same case studies, as the TSLS-PSS uses a conservative approximation of the limiters and employs a discretization with fixed steps. We validate the TSLS-PSS model on coarser and fine discretization steps

TABLE III

RESULTS FOR THE RANGE-RESTRICTED TSLS-PSS MODEL: DISPATCH DISTANCE (MW/MVAR), COST DIFFERENCE (\$), AND RUNTIME (SEC).

Congestion (%)	No dispatch change: $r = 0\%$, $\gamma = 0.2\%$			
	Line	Dispatch dist.	Cost diff.	Runtime
50	(4,14)	0.00/0.00	0.00 (0.00%)	712.41
70	(16,17)	0.00/0.00	0.00 (0.00%)	169.03
80	(16,17)	0.00/0.00	0.01 (0.00%)	350.82
85	(2,25)	0.00/0.00	0.00 (0.00%)	117.08
88	(2,25)	0.00/0.00	0.00 (0.00%)	616.84
90	No SW ⁴	Converge Err.	-	-

TABLE IV

RUNTIME (SEC), GENERATION COST DIFFERENCE (%), AND ERRORS (DEG), WITH NO DISPATCH CHANGE ($r = 0\%$, $\gamma = 0.2\%$)

Time step (sec)	Model var. num.	85%			88%		
		Error	Cost diff.	Runtime	Error	Cost diff.	Runtime
0.160	14,473	0.003	0.00%	64.27	0.009	0.00%	106.95
0.125	18,246	0.002	0.00%	59.04	0.005	0.00%	389.87
0.080	27,948	0.001	0.00%	117.08	0.002	0.00%	616.84
0.040	54,898	0.001	0.00%	203.10	0.003	0.00%	4979.84

ranging from 0.160s to 0.040s. Transient simulations in PowerWorld are run with the second order Runge-Kutta integration method (RK) with 10^{-3} second step size. PowerWorld is known to have potential numerical issues when time constant parameters are too small or gains are too large [30]. These difficulties were encountered in the case study when the lead-lag ratios T_1/T_3 or T_2/T_4 were large. To circumvent this difficulty, we added a constraint in the model to restrict the max ratio to 60. Table III updates the previous results with the additional restriction. The results are similar in nature to the earlier results.

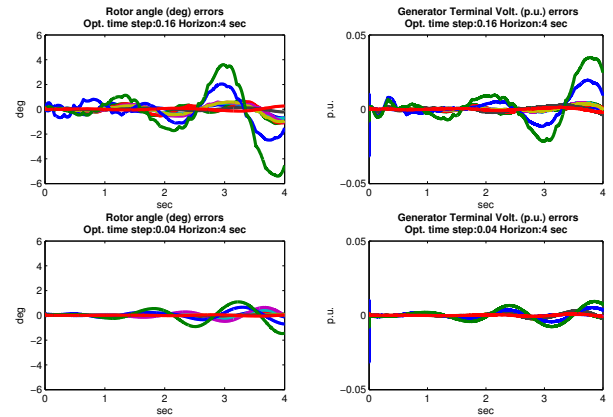


Fig. 6. Error functions on rotor angles (deg) and terminal voltages (p.u.) for 88% congestion ($r = 0\%$, $\gamma = 0.2\%$) and discretization steps of 0.160s (top) and 0.040s (bottom).

We are now in a position to compare the TSLS-PSS model and the simulation results seeded with the generator dispatch and AVR values found by the optimization model. The results are given in Table IV which, for each time step, reports the number of variables in the optimization, the CPU runtime (sec), the cost difference (in %), and a metric to measure the accuracy of the optimization results with respect to the simulation outcomes. The accuracy metric is expressed in terms of $\delta_s^n(t)$ and $\delta_o^n(t)$ which denote the rotor angle obtained by the simulation and the (interpolated) rotor angle obtained by optimization for generator n at simulated time

$t \in T^s$ respectively. It computes the average errors (L2 norm) on the rotor angles (deg), i.e.,

$$\frac{1}{|G||T^s|} \sum_{n \in G} \sqrt{\sum_{t \in T^s} [\delta_s^n(t) - \delta_o^n(t)]^2}$$

This accuracy metric represents the average errors of rotor angles in degrees, per generator machine and time point. Figure 6 shows also four error plots that report the difference between optimization and simulation on rotor angles (deg.) and generator terminal voltages (p.u.) for the 88% cases. Table IV and Figure 6 show the TSLs-PSS model has high accuracy with respect to simulation, with an average error in the scale of 10^{-3} deg. The error functions further show finer discretization decrease the worst-case error to 2 deg.

VII. CONCLUSION

This paper proposed an automatic control and optimization routine to address transient stability during transmission line switchings in highly congested situations. The optimization model is based on trapezoidal discretization on the differential equations for the 2-axis generator model with an AVR circuit, and uses the stability/exciter parameters as control variables to drive the system towards transient stability. In particular, the objective function minimizes the sum of the time-weighted rotor angle accelerations, to ensure increasingly smaller swings as time increases. Experimental results show that the PSS parameters are critical in damping the system to ensure long-term stability and that the test cases can be solved within minutes for the IEEE 10-machine 39 bus system. The model was validated against the PowerWorld simulator and is shown to have an accuracy in the order of 10^{-3} (average degree error) in rotor angle computations. Future work includes studying on a longer horizon to guarantee stability and implementing higher order models.

ACKNOWLEDGMENT

We thank the editors and reviewers for their constructive comments and suggestions. Terrence W.K. Mak was supported by Data61/CSIRO, funded by the Australian Government through the ICT Centre of Excellence Program.

REFERENCES

- [1] C. Coffrin, H. Hijazi, K. Lehmann, and P. Van Hentenryck, "Primal and dual bounds for optimal transmission switching," in *Proceedings of the 18th Power Systems Computation Conference (PSCC'14)*, 2014.
- [2] T. Potluri and K. W. Hedman, "Impacts of topology control on the acopf," in *2012 IEEE Power and Energy Society General Meeting*, July 2012, pp. 1–7.
- [3] E. B. Fisher, R. P. O'Neill, and M. C. Ferris, "Optimal transmission switching," *IEEE Transactions on Power Systems*, vol. 23, no. 3, pp. 1346–1355, Aug 2008.
- [4] W. Shao and V. Vittal, "Corrective switching algorithm for relieving overloads and voltage violations," *IEEE Transactions on Power Systems*, vol. 20, no. 4, pp. 1877–1885, Nov 2005.
- [5] K. W. Hedman, R. P. O'Neill, E. B. Fisher, and S. S. Oren, "Optimal transmission switching - sensitivity analysis and extensions," *IEEE Transactions on Power Systems*, vol. 23, no. 3, pp. 1469–1479, Aug 2008.
- [6] J. D. Fuller, R. Ramasra, and A. Cha, "Fast heuristics for transmission-line switching," *IEEE Transactions on Power Systems*, vol. 27, no. 3, pp. 1377–1386, Aug 2012.
- [7] C. Barrows and S. Blumsack, "Transmission switching in the rts-96 test system," *IEEE Transactions on Power Systems*, vol. 27, no. 2, pp. 1134–1135, May 2012.
- [8] C. Barrows, S. Blumsack, and R. Bent, "Computationally efficient optimal transmission switching: Solution space reduction," in *2012 IEEE Power and Energy Society General Meeting*, July 2012, pp. 1–8.
- [9] K. W. Hedman, S. S. Oren, and R. P. O'Neill, *Flexible Transmission in the Smart Grid: Optimal Transmission Switching*. Berlin, Heidelberg: Springer Berlin Heidelberg, 2012, pp. 523–553.
- [10] M. Soroush and J. D. Fuller, "Accuracies of optimal transmission switching heuristics based on dcofp and acopf," *IEEE Transactions on Power Systems*, vol. 29, no. 2, pp. 924–932, March 2014.
- [11] T. Athay, R. Podmore, and S. Virmani, "A practical method for the direct analysis of transient stability," *IEEE Transactions on Power Apparatus and Systems*, vol. PAS-98, no. 2, pp. 573–584, 1979.
- [12] M. Pai, *Energy function analysis for power system stability*. Springer US, 1989.
- [13] C. Coffrin, D. Gordon, and P. Scott, "Nesta, the NICTA energy system test case archive," *CoRR*, vol. abs/1411.0359, 2014. [Online]. Available: <http://arxiv.org/abs/1411.0359>
- [14] D. Gan, R. Thomas, and R. Zimmerman, "Stability-constrained optimal power flow," *IEEE Transactions on Power Systems*, vol. 15, no. 2, pp. 535–540, May 2000.
- [15] Y. Yuan, J. Kubokawa, and H. Sasaki, "A solution of optimal power flow with multicontingency transient stability constraints," *Power Systems, IEEE Transactions on*, vol. 18, no. 3, pp. 1094–1102, Aug 2003.
- [16] H. Hijazi, T. W. K. Mak, and P. Van Hentenryck, "Power system restoration with transient stability," in *AAAI'15*, 2015.
- [17] N. Martins, E. De Oliveira, W. Moreira, J. L. R. Pereira, and R. Fontoura, "Redispatch to reduce rotor shaft impacts upon transmission loop closure," *IEEE Transactions on Power Systems*, vol. 23, no. 2, pp. 592–600, 2008.
- [18] H. Ye and Y. Liu, "A new method for standing phase angle reduction in system restoration by incorporating load pickup as a control means," *International Journal of Electrical Power & Energy Systems*, vol. 53, pp. 664–674, 2013.
- [19] D. Hazarika and A. Sinha, "An algorithm for standing phase angle reduction for power system restoration," *IEEE Transactions on Power Systems*, vol. 14, no. 4, pp. 1213–1218, 1999.
- [20] "Powerworld simulator," PowerWorld Corporation, <http://www.powerworld.com>.
- [21] P. Kundur, N. J. Balu, and M. G. Lauby, *Power system stability and control*. McGraw-hill New York, 1994.
- [22] P. Sauer and M. Pai, *Power System Dynamics and Stability*. Stipes Publishing L.L.C., 2006.
- [23] R. Zimmerman, C. Murillo-Sanchez, and R. Thomas, "MATPOWER: Steady-state operations, planning, and analysis tools for power systems research and education," *IEEE Transactions on Power Systems*, vol. 26, no. 1, pp. 12–19, feb. 2011.
- [24] I. Hiskens, "IEEE PES task force on benchmark systems for stability controls (39 bus system MATLAB report)," IEEE PES Power System Dynamic Performance Committee, Tech. Rep., Nov 2013, accessed 13 July 2016: [http://eioc.pnnl.gov/benchmark/ieees/IEEE39/New_England.Reduced.Model.\(39_bus_system\).MATLAB_study_report.pdf](http://eioc.pnnl.gov/benchmark/ieees/IEEE39/New_England.Reduced.Model.(39_bus_system).MATLAB_study_report.pdf).
- [25] R. Fourer, D. M. Gay, and B. W. Kernighan, *AMPL: A Modeling Language for Mathematical Programming*. Cengage Learning, 2002.
- [26] P. Bonami, L. T. Biegler, A. R. Conn, G. Cornujols, I. E. Grossmann, C. D. Laird, J. Lee, A. Lodi, F. Margot, N. Sawaya, and A. Wächter, "An algorithmic framework for convex mixed integer nonlinear programs," *Discrete Optimization*, vol. 5, no. 2, pp. 186–204, 2008.
- [27] "A collection of Fortran codes for large scale scientific computation," <http://www.hsl.rl.ac.uk/>, 2016.
- [28] A. Wächter and L. T. Biegler, "On the implementation of an interior-point filter line-search algorithm for large-scale nonlinear programming," *Mathematical Programming*, vol. 106, no. 1, pp. 25–57, 2006.
- [29] S. M. Baek, J. W. Park, and I. A. Hiskens, "Optimal tuning for linear and nonlinear parameters of power system stabilizers in hybrid system modeling," *IEEE Transactions on Industry Applications*, vol. 45, no. 1, pp. 87–97, Jan 2009.
- [30] B. Gang, "Columbia Grid transient stability manual," Columbia Grid, Tech. Rep., April 2016, accessed 2 Aug 2016: <https://www.columbiagrid.org/TransientStability-overview.cfm>.